
KSP MIDTERM REPORT

Nirav Bhattad

Last updated June 22, 2024

Contents

1	Introduction to Radio Astronomy	1
1.1	Introduction	1
1.2	Historical Development and Milestones	2
1.3	Fundamentals of Radio Waves	4
1.4	Sky Coordinate System	7
1.5	Radio Telescopes	10
1.6	Radio Maps	11
1.7	Galaxy FITS Data in Multiple Wavelengths	14
1.8	Jet Afterglow Lightcurve of GW170817	16
2	Introduction to Radiation Physics	17
2.1	Measuring Radiation	17
2.2	Blackbody Radiation	18
2.3	Rayleigh-Jeans Approximation	20
2.4	Brightness Temperature	22
2.5	Coherent Radiation	23
2.6	Interference of Light	24
2.7	Polarization of Light	25
2.8	Cosmic Microwave Background	26
2.9	Hydrogen 21cm Line & Galaxy Rotation Curve	27
3	Radio Telescopes	29

Chapter 1

Introduction to Radio Astronomy

§1.1. Introduction

Radio astronomy involves the study of radio waves from the depths of space. Many objects in the universe emit radio waves through naturally occurring processes. Such objects include stars, galaxies, and nebulae, as well as a wide variety of peculiar, fascinating, and often mysterious objects, such as pulsars and quasars. Radio astronomers study such objects using a variety of radio telescopes. Many of the astronomical objects that emit radio waves do not emit much or any light so that radio astronomers study what is essentially an invisible universe not seen by even the world's largest optical telescopes.

The development of radio astronomy in the mid-twentieth century opened a new window on the universe. Before this development, astronomical observations were confined to the narrow range of visible wavelengths, limiting the range of astronomical phenomena that could be studied. The sky at radio wavelengths is vastly different from the sky observed in visible light. Stars, which are the primary sources of visible light, do not dominate the emission in the radio sky.

At radio wavelengths, we can detect thermal continuum and spectral-line emission from objects too cold to emit visible light. This enables the study of the cold interstellar medium of our Galaxy and others, as well as the cosmic microwave background, the relic radiation from the early universe. Nonthermal radiation, such as synchrotron emission, produces significant radio emission and is observed in a variety of astronomical sources like supernova remnants and quasars. For instance, two of the brightest sources in the radio sky, Cassiopeia A and Cygnus A, are synchrotron-emitting sources that are relatively faint at visible wavelengths. Thus, radio observations complement optical observations.

§1.2. Historical Development and Milestones

The field of radio astronomy began in the early 20th century, revolutionizing our understanding of the universe by exploring it beyond visible wavelengths. The foundation for radio astronomy was laid in the 19th century through advances in electricity and magnetism, particularly with Maxwell's equations, which revealed the vast spectrum of electromagnetic radiation.

1.2.1. Early Efforts and Discoveries

In 1887, Heinrich Hertz successfully produced radio waves in a laboratory, sparking interest in detecting cosmic radio waves. Pioneering efforts in the 1890s by Thomas Edison, Arthur Kennelly, and Sir Oliver Lodge to find correlations between sunspots and radio signals failed due to the insensitivity of the equipment used. Other astronomers like Johannes Wilsing, Julius Scheiner, and Charles Nordmann also faced similar setbacks.

1.2.2. Breakthroughs in the 1930s

The critical advancement came in 1932 when Karl Jansky of Bell Labs successfully detected astronomical radio emissions while studying static interference in short-wave radio communications. Using a steerable antenna, Jansky identified a steady hiss with a directional dependence, tracing it to the plane of the Milky Way and pinpointing the galactic center as a primary source. His work, however, initially received little attention.

Intrigued by Jansky's findings, Grote Reber, an engineer, constructed a 30-foot parabolic antenna in his backyard in 1937. After initial failures at higher frequencies, Reber succeeded in mapping the galaxy's radio emissions at 160 MHz. His detailed maps identified significant sources, including the strong emission from the galactic center and secondary peaks in Cassiopeia (Cas A) and Cygnus (Cyg A). Reber's work, published in 1940 and 1944, marked the first radio wavelength observations in an astronomical journal.

1.2.3. Advancements During and After World War II

World War II brought significant technological advancements in radar, leading to critical developments in radio astronomy. In 1942, J.S. Hey of the British Army Operational Research Group linked radar jamming to sunspot activity, a hypothesis later supported by Southworth of Bell Labs, who detected radio emissions from the quiescent Sun.

Post-war, Hey and colleagues continued their radio studies, discovering in 1945 that meteor trails reflect radio waves and mapping the radio sky in greater detail than Reber. They identified Cygnus A as a discrete source and in 1948 linked solar radio bursts to sunspots and solar flares.

1.2.4. The Hydrogen Line and Interferometry

In 1944, Dutch astrophysicist Jan Oort suggested to Hendrik van de Hulst the calculation of the hydrogen emission line due to electron spin-flip transitions. Van de Hulst predicted radiation at a 21-cm wavelength, first detected by Harold Ewen and Edward Purcell at Harvard in 1951. This discovery enabled detailed hydrogen mapping in the Milky Way and remains a vital tool in radio astronomy.

In 1946, Martin Ryle and D.D. Vonberg conducted the first interferometric observations using paired radio antennas. Subsequent interferometry by various researchers provided precise positions for bright radio sources, facilitating optical identifications of objects like Cygnus A, Cassiopeia A, and the Crab Nebula. By 1959, the Third Cambridge Catalog (3C) cataloged the brightest 471 radio sources, later revised as 3CR.

1.2.5. Theoretical Insights and Nobel Prizes

The 1950s saw the understanding of synchrotron radiation, a process where relativistic electrons emit photons while spiraling around magnetic field lines, proposed by Hannes Alfvén, Nicolai Herlofsen, and Iosif Shklovsky. The 1960s brought significant discoveries, including quasars, pulsars, and the cosmic microwave background (CMB). These

discoveries led to several Nobel Prizes: the 1974 prize to Anthony Hewish for the discovery of pulsars and the 1978 prize to Arno Penzias and Robert Wilson for the CMB. Further studies on pulsars and the CMB earned additional Nobel Prizes in 1993 (Joseph Taylor and Russell Hulse) and 2006 (John Mather and George Smoot).

§1.3. Fundamentals of Radio Waves

This section provides a basic introduction to radio waves and electromagnetic radiation, essential for understanding radio astronomy.

1.3.1. Electromagnetic Radiation

Radio waves are a form of electromagnetic (EM) radiation, similar to visible light but at much lower frequencies. EM radiation consists of oscillating electric and magnetic fields that are perpendicular to each other and to the direction of propagation (Figure 1.1).

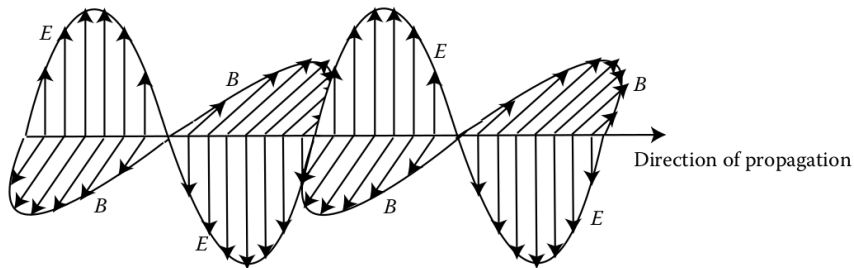


Figure 1.1: Waves of electromagnetic radiation.

The speed of EM waves in a vacuum is the speed of light, $c = 299792458$ m/s. The frequency, ν , in hertz (Hz), and the wavelength, λ , in meters, are related by

$$\lambda\nu = c \quad (1.3.1)$$

EM waves are often generated by accelerating charged particles, typically electrons due to their smaller mass compared to protons. Light can be described both as a wave and as a particle (photon). The energy of a photon is given by

$$E = h\nu = \frac{hc}{\lambda} \quad (1.3.2)$$

where h is Planck's constant, $h = 6.626 \times 10^{-34}$ J s. The electromagnetic spectrum covers a wide range of frequencies and wavelengths (Figure 1.2).

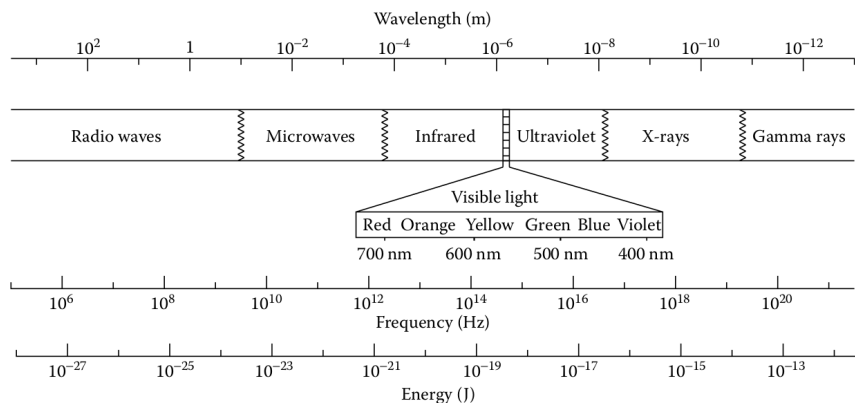


Figure 1.2: The electromagnetic spectrum.

The radio band spans from 10 MHz to 300 GHz (30 m to 1 mm in wavelength). The Earth's atmosphere allows radio waves within this range to reach the surface, except at very low frequencies (below 10 MHz) and high frequencies (above 300 GHz) due to ionospheric and atmospheric absorption.

1.3.2. Spectroscopy

Spectroscopy involves analyzing the spectrum (intensity vs. frequency or wavelength) of detected radiation, providing valuable information about the source. Classical spectrographs use prisms or gratings to separate wavelengths (Figure 1.3).

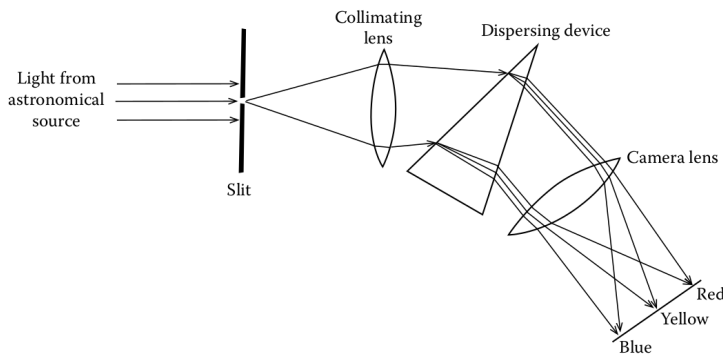


Figure 1.3: A classical spectrograph setup.

Radio spectrographs separate frequencies electronically, displaying the spectrum as intensity vs. frequency. There are three types of spectra based on Kirchhoff's rules:

1. **Continuous spectra:** Emission at all frequencies without breaks. An example is an incandescent lamp (Figure 1.4).

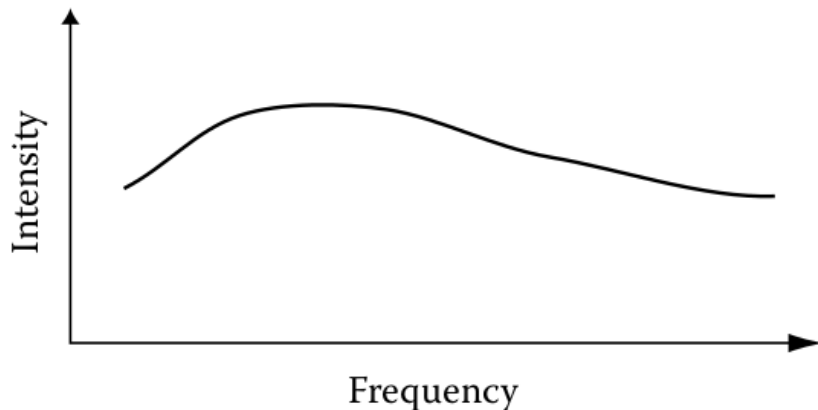


Figure 1.4: Qualitative example of a continuous spectrum.

2. **Emission line spectra:** Emission at specific frequencies due to quantum transitions in atoms or molecules (Figure 1.5).

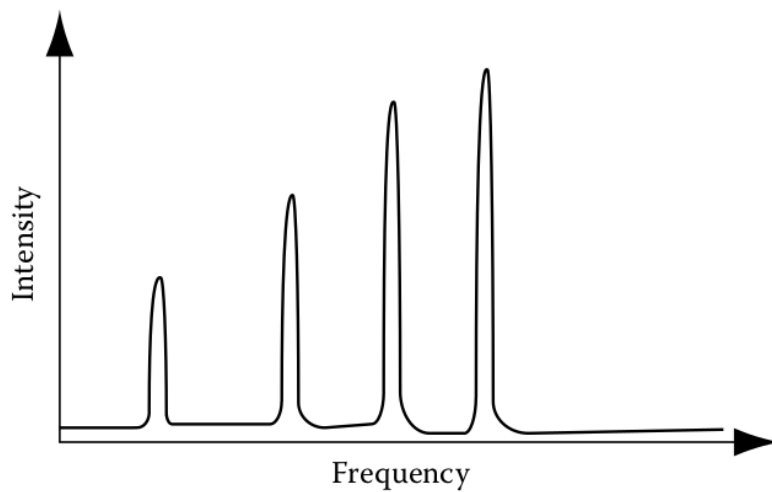


Figure 1.5: Qualitative sketch of an emission line spectrum.

3. **Absorption line spectra:** Dark lines appear when radiation passes through a cooler gas, which absorbs specific frequencies (Figure 1.6).

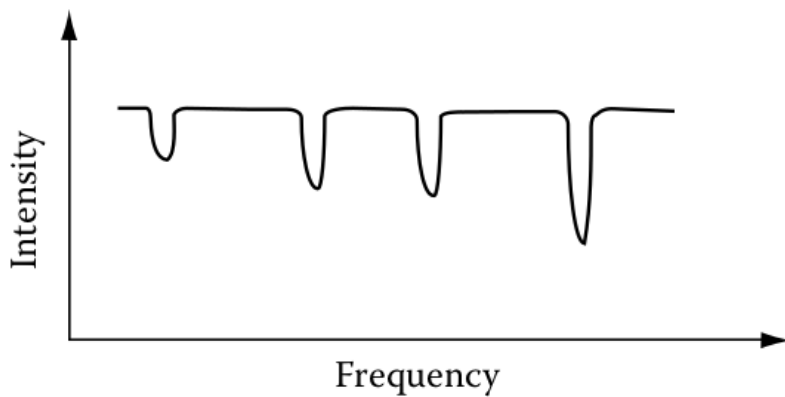


Figure 1.6: Qualitative example of an absorption line spectrum.

The specific frequencies of emission and absorption lines allow identification of the chemical composition of the source or intervening gas.

§1.4. Sky Coordinate System

1.4.1. Right Ascension and Declination

To locate objects in the sky, we use a coordinate system similar to Earth's. The celestial sphere, an imaginary globe surrounding Earth, uses extensions of longitude (right ascension, RA, α) and latitude (declination, Dec, δ) lines. The celestial poles align with Earth's poles, and the sky appears to rotate about an axis through these poles.

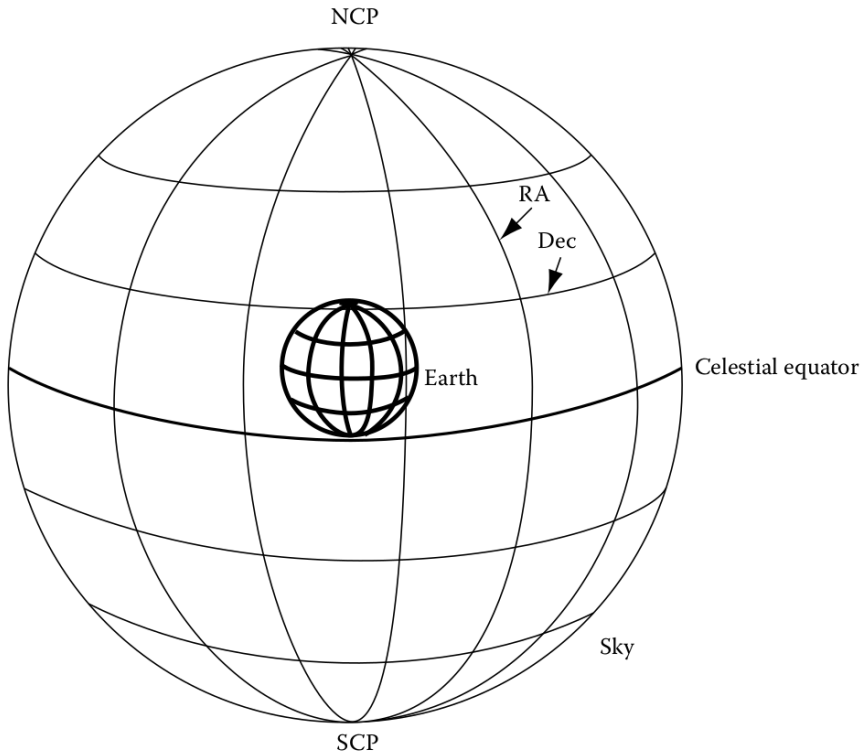


Figure 1.7: The celestial sphere with RA and Dec lines.

Declination is analogous to latitude and is measured in degrees from the celestial equator. RA, fixed relative to the stars, is defined such that the 0° line of RA aligns with the 0° line of longitude at noon on the first day of spring. RA is measured in hours, minutes, and seconds, with 24 h of RA corresponding to 360° .

The units of RA are time-based due to historical reasons and simplify calculations involving Earth's rotation. The conversion between RA and degrees at the equator is $1\text{ h RA} = 15^\circ \text{ arc}$, $1\text{ min RA} = 15 \text{ min arc}$, and $1\text{ s RA} = 15 \text{ s arc}$. Away from the equator, the angular separation between RA lines depends on declination (δ) and is given by:

$$\text{Seconds of arc} = 15 \cos(\delta) \times \text{seconds of RA}$$

On sky maps, east appears to the left, and RA increases to the left, due to the observer's perspective relative to the ground.

1.4.2. Observer-Centered Definitions

1. **Horizon:** The boundary of visible sky, blocked by the ground.
2. **Zenith:** The point directly overhead.
3. **Altitude/Elevation:** Angular height above the horizon (0° at horizon, 90° at zenith).

4. **Azimuth:** Angular position along the horizon from north (0° north, 180° south, 90° east, 270° west).

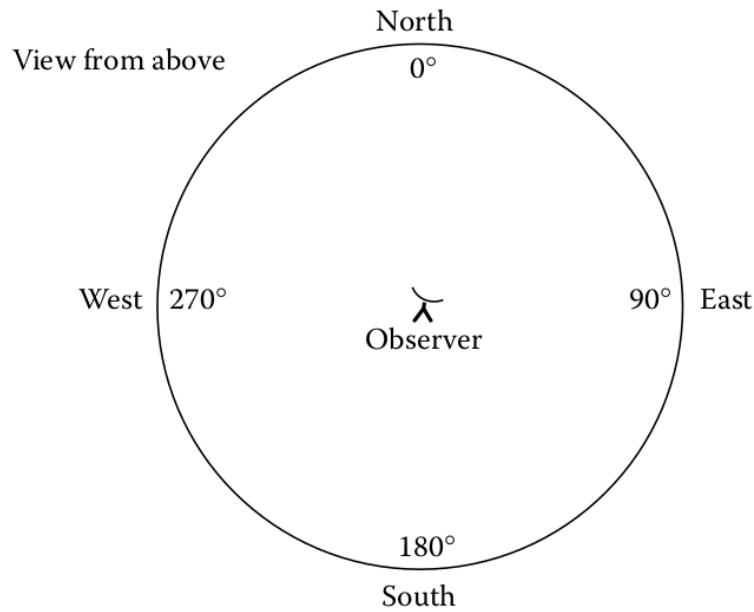


Figure 1.8: View from above depicting azimuthal angles along with the cardinal directions around the horizon.

5. **Meridian:** The line of RA through your zenith, connecting to celestial poles.

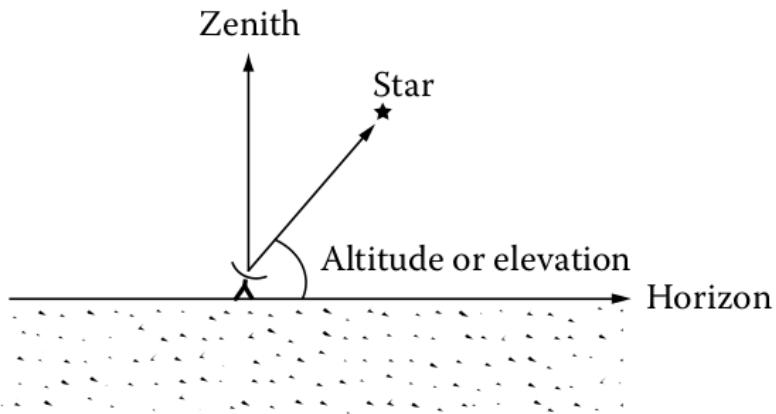


Figure 1.9: Schematic diagram showing the relations between zenith, horizon, and altitude or elevation.

6. **Transit:** When an object crosses your meridian, highest in the sky.
7. **Hour Angle (HA):** Hours since an object crossed your meridian.
8. **Local Sidereal Time (LST):** RA currently on your meridian, running slightly faster than solar time. ($HA = LST - RA$)
9. **Universal Time (UT):** Local solar time at Greenwich, England, standardized for timekeeping.

RA measured in time simplifies finding when objects cross the meridian and explains its increase to the east.

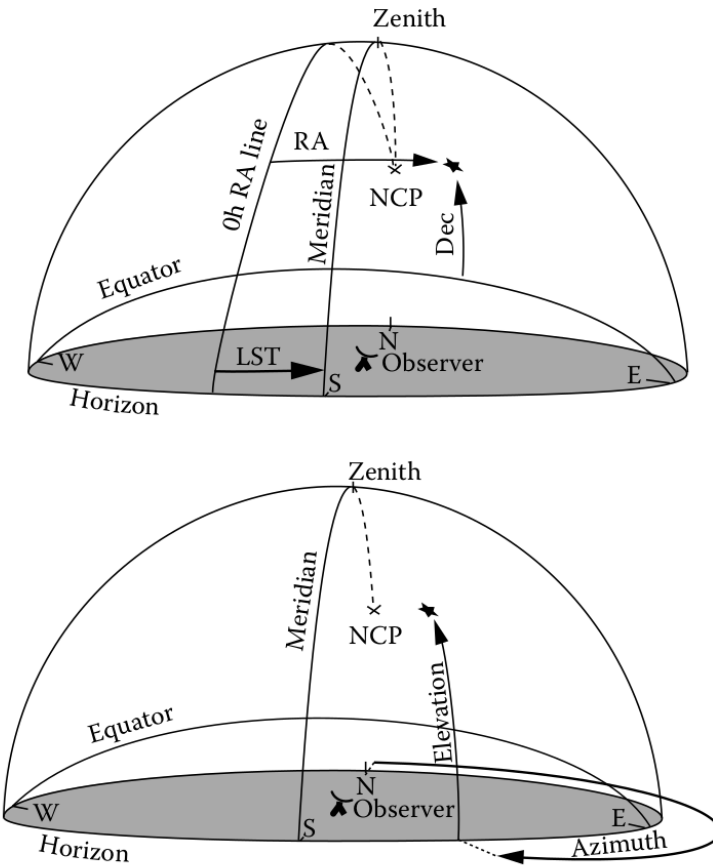


Figure 1.10: Example of sky coordinates as viewed by the observer (top) and observer-centered coordinates (bottom).

1.4.3. Apparent Sizes

Angular size, dependent on an object's actual size and distance, is measured in radians:

$$\theta \text{ (radians)} = \frac{s}{r}$$

For small angles:

$$\theta \text{ (radians)} \approx \frac{l}{d}$$

In two dimensions, the solid angle Ω is:

$$\Omega = \frac{A}{d^2}$$

with the unit steradian (sr), and the whole sky covering 4π sr.

Understanding these coordinate systems allows us to locate and observe celestial objects from any Earth location and describe their apparent positions and sizes accurately.

§1.5. Radio Telescopes

Observing with a radio telescope differs significantly from using a visible-wavelength telescope. The Sun does not illuminate the entire sky at radio wavelengths, resulting in a dark daytime sky suitable for observations day and night. Long radio wavelengths penetrate clouds, whereas shorter wavelengths require clear skies due to water-induced signal loss.

A traditional radio telescope comprises five basic parts.

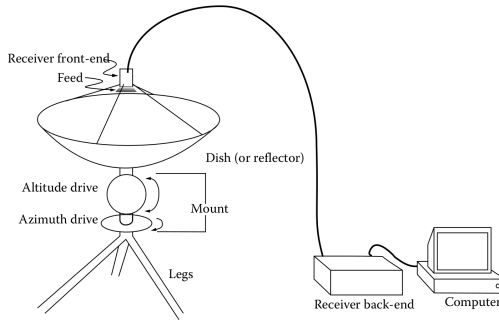


Figure 1.11: A schematic diagram of a radio telescope.

1.5.1. Parabolic Reflector

Most radio telescopes use a parabolic reflector (dish) to collect and focus radio waves. Unlike visible-light telescopes, radio telescopes do not use lenses. The radiation can be detected at the focal point (prime focus) or behind the dish (Cassegrain focus).

1. The sensitivity of the telescope depends on the collecting area, proportional to the square of the reflector's diameter.
2. Radio dishes do not need highly polished surfaces. Successful reflection occurs when surface irregularities are much smaller than the wavelength, $\delta z < \frac{\lambda}{20}$. For longer wavelengths, the surface can be a mesh.
3. The resolution of a radio telescope is determined by diffraction, improving with larger reflectors.

1.5.2. Mount

The mount holds and moves the dish, allowing rotation around two axes. Modern radio telescopes use altitude-azimuth (Alt-Az) mounts, while older visible-wavelength telescopes often use equatorial mounts.

1.5.3. Feeds, Receivers, and Computer

The dish focuses radio waves to feeds that convert them into transmission lines, sending signals to receivers. The receiver front-end amplifies and processes the signal, which is then transmitted to the observatory's control room for further processing by the back-end and storage on a computer.

Each feed-receiver assembly acts like a pixel. Radio telescopes typically have fewer feed-receiver assemblies compared to the megapixel arrays in visible-wavelength telescopes due to the larger size and cost. Large telescopes like Arecibo and Green Bank can have 7 to 13 assemblies, while smaller ones like Haystack SRT have only one. At millimeter wavelengths, arrays with thousands of bolometer detectors exist.

Radio observations often yield fewer data points compared to visible-wavelength observations, but aperture synthesis (combining signals from multiple telescopes) can produce detailed images.

§1.6. Radio Maps

Displaying the structure of a source at radio wavelengths requires choosing the best way to present two-dimensional data. There are three common approaches:

1.6.1. Contour Maps

The simplest way is using a contour map, where contours are lines of constant intensity, similar to a topographical map indicating lines of constant elevation. Closely spaced contours indicate regions where the intensity changes rapidly. An example of a contour map is shown in Figure 1.12.

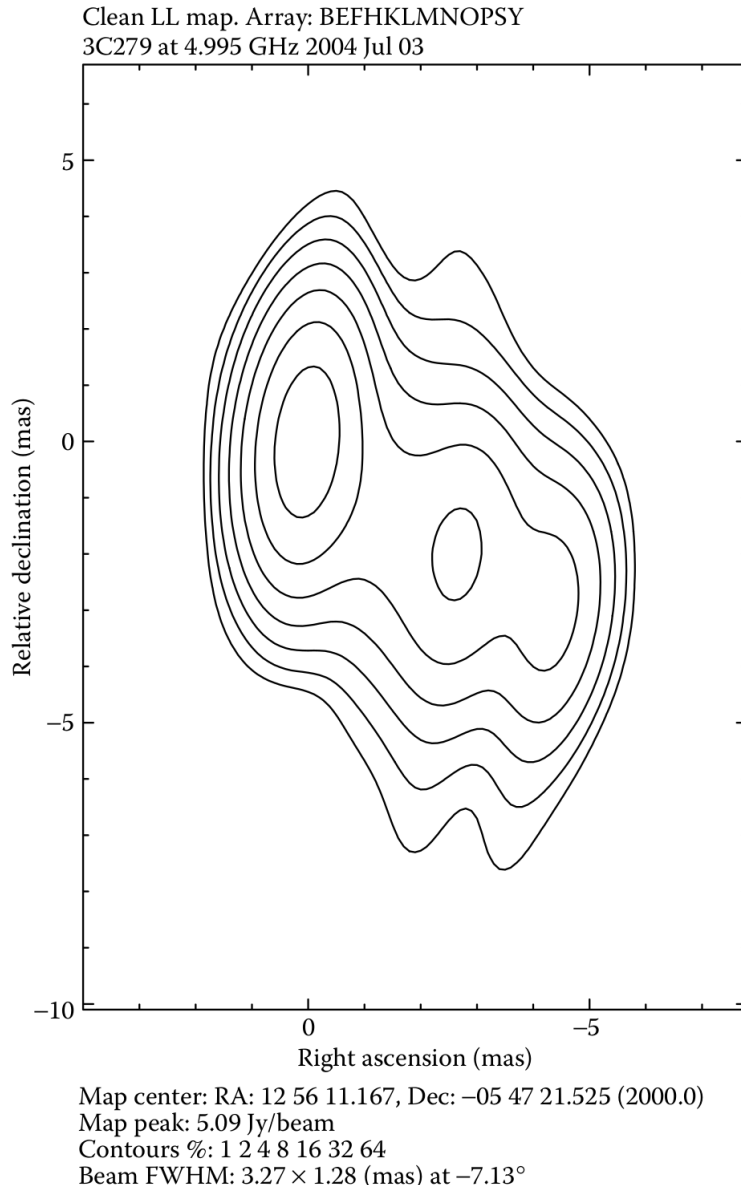


Figure 1.12: An example of a contour map.

1.6.2. Gray Scale Maps

A gray scale map directly indicates brightness variations with shades of gray, where black is the most intense and white the least. Although gray scale maps are more intuitive, they often do not reveal details as well as contour maps. Therefore, contour maps are preferred for detailed analysis. Overlaid gray scale and contour maps, as shown in Figure 1.13, are common and visually pleasing.

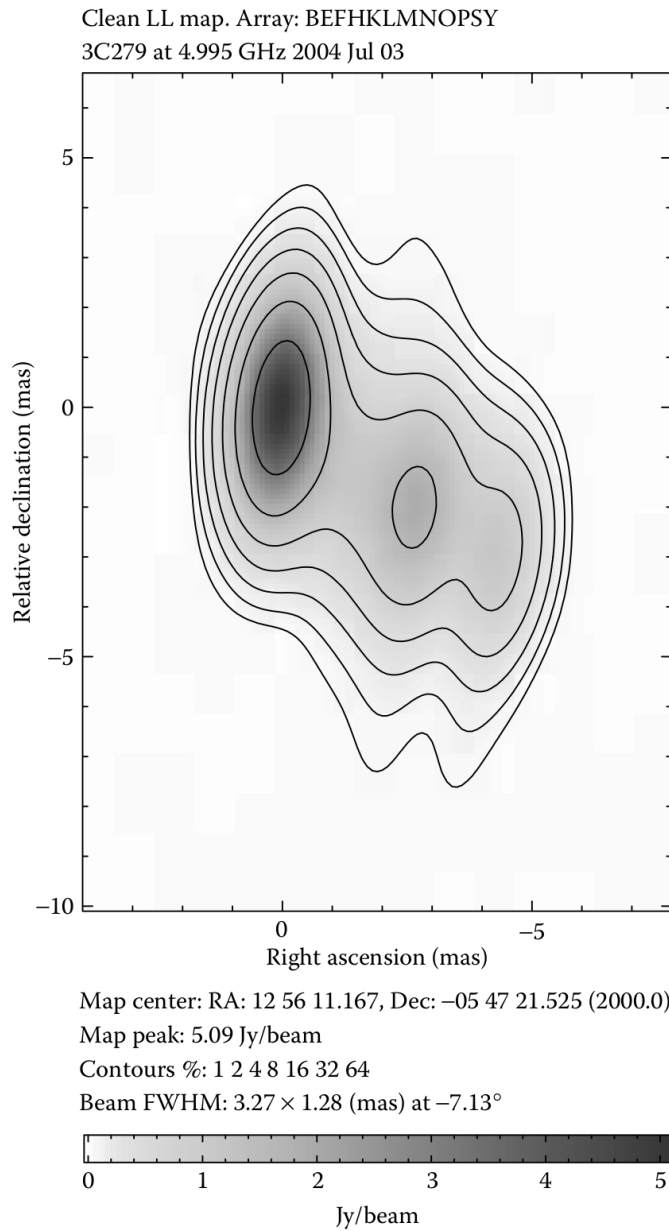


Figure 1.13: An example of an overlaid gray scale and contour map.

1.6.3. False Color Maps

False color maps use colors to indicate different levels of brightness rather than wavelengths. These images often include a color-wedge to show the relationship between color and brightness, facilitating analysis. An example of a false color map is shown in Figure 1.14.

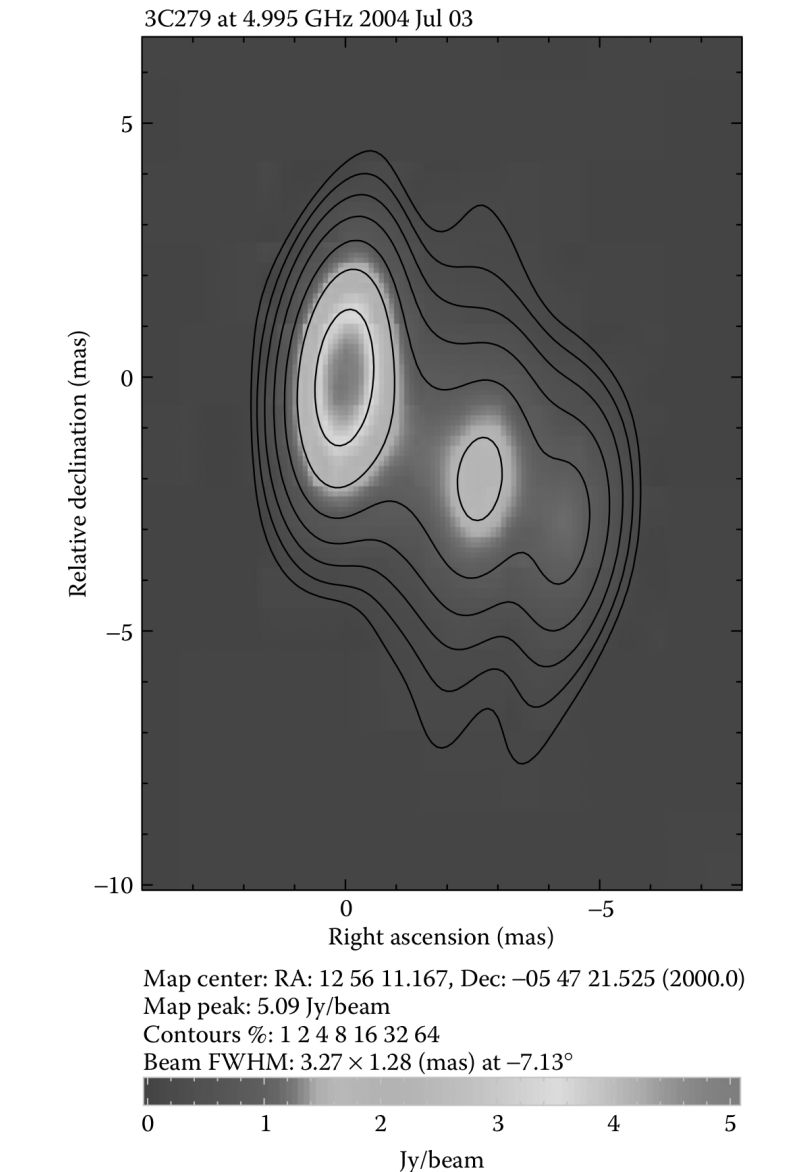


Figure 1.14: An example of a false color map.

1.6.4. Multicolor Images

Radio astronomers sometimes create multicolor images similar to visible light astronomers. By observing several different radio wavelengths, images can be overlaid, assigning red to the longest wavelength, green to intermediate wavelengths, and blue to the shortest wavelength.

§1.7. Galaxy FITS Data in Multiple Wavelengths

We will choose 3 Galaxies - Sunflower, Tadpole and Whirlpool Galaxy, and use the CIRADA [CIR24] image cutout web service to display their FITS [NAS24] data in multiple wavelengths. This service enables us to obtain optical, infrared, and radio images of all three galaxies.

Different wavelengths reveal different aspects of the galaxies. Optical images show the distribution of stars, while infrared images reveal the distribution of dust and gas. Radio images show the distribution of cold gas and synchrotron radiation from cosmic rays.

1.7.1. Sunflower Galaxy

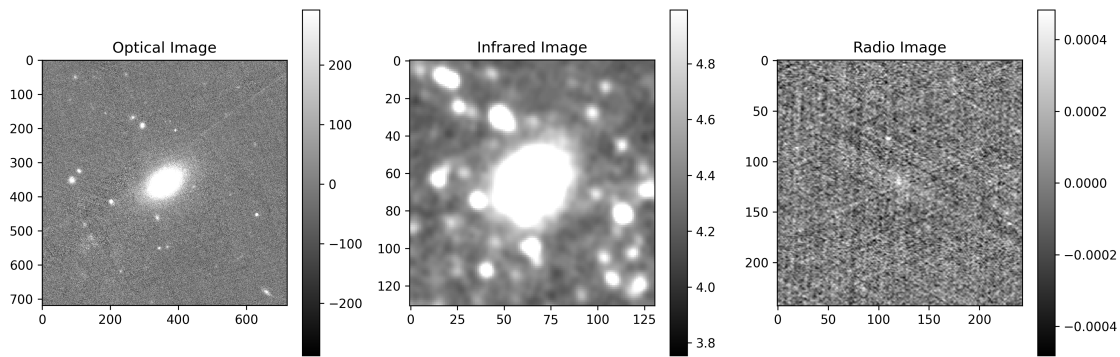


Figure 1.15: Sunflower Galaxy in multiple wavelengths.

1.7.2. Tadpole Galaxy

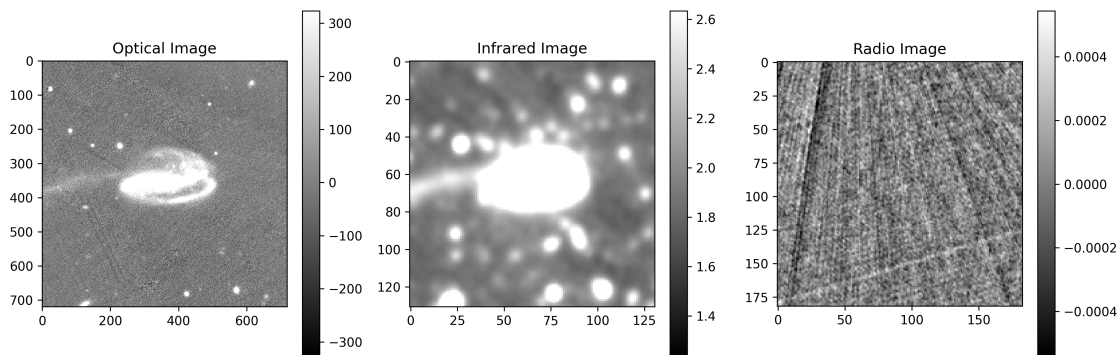


Figure 1.16: Tadpole Galaxy in multiple wavelengths.

1.7.3. Whirlpool Galaxy

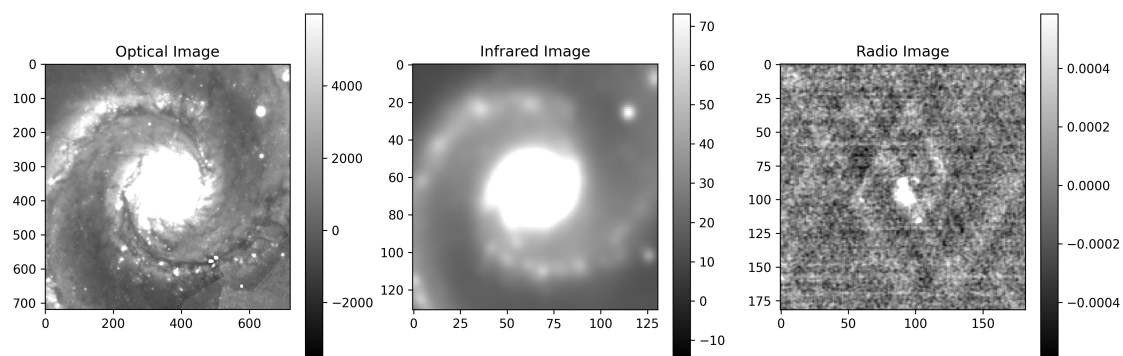


Figure 1.17: Whirlpool Galaxy in multiple wavelengths.

§1.8. Jet Afterglow Lightcurve of GW170817

GW170817 [Kc24] was a merger of two neutron stars that was accompanied by both gravitational waves and electromagnetic radiation. We used the data for the non-thermal emission from this source that spans across all frequency bands following a single spectral index of $F_\nu \propto \nu^{-0.584}$. The quantity F is the flux density, which measures the amount of energy incident on the detector per unit area of the detector, an indicator of the brightness of the source. A lightcurve is this flux density represented as a function of time.

We plotted the lightcurve choosing all the VLA 3 GHz data points.

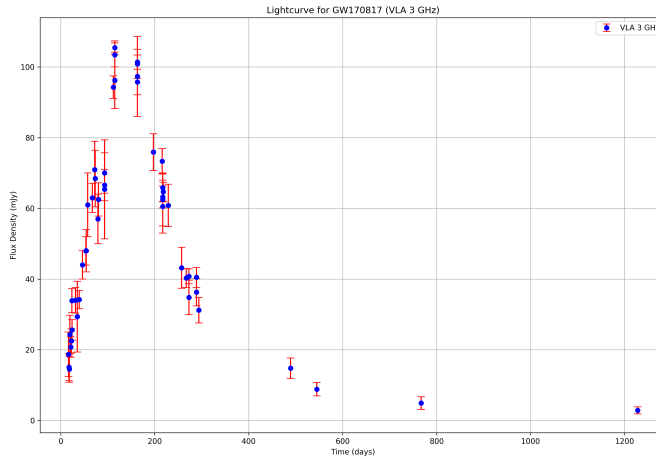


Figure 1.18: Flux Density vs Time at 3GHz frequency measured by VLA telescope.

We also plotted the lightcurve choosing all the Chandra 3 GHz data points.

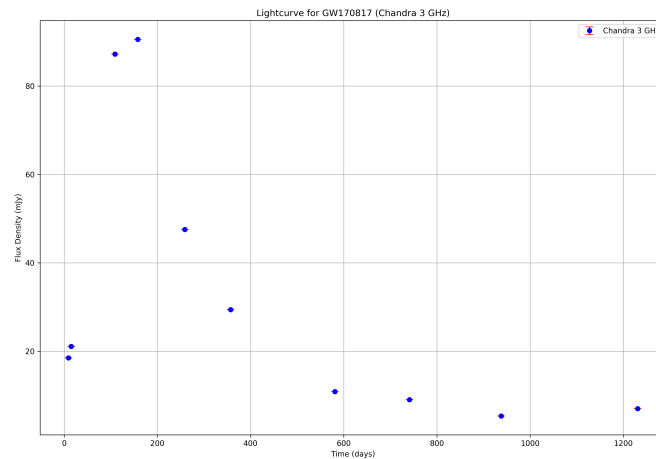


Figure 1.19: Flux Density vs Time at 3GHz frequency measured by Chandra telescope.

Chapter 2

Introduction to Radiation Physics

§2.1. Measuring Radiation

One quantitative measure that astronomers use when observing a light source is the amount of radiation received. Quantifying this amount involves several related but distinct concepts. We discuss these measures below.

2.1.1. Total Energy Emitted

A source's total light output can be described by the total amount of energy emitted over its lifetime, at all frequencies, and in all directions. However, this comprehensive measure is impractical for direct observation since we can only measure radiation over finite time periods. Instead, we focus on measurements normalized by time.

2.1.2. Luminosity

Luminosity (L) or power is the rate at which energy is emitted by a source, expressed in watts (W) or ergs per second (erg s⁻¹). It is calculated by dividing the total emitted energy by the time period over which it was emitted.

2.1.3. Flux

Flux (F) measures the amount of light energy per unit time per unit area that we detect from a source. It is normalized by dividing the detected power by the effective area of the telescope receiving the radiation. Flux is expressed in units of joules per second per square meter (J s⁻¹ m⁻²) or watts per square meter (W m⁻²).

The relationship between flux and luminosity for an isotropic source at distance d is given by:

$$F = \frac{L}{4\pi d^2}$$

2.1.4. Flux Density

Flux density (F_ν or F_λ) refers to the flux per unit frequency or wavelength range observed. It is calculated by dividing the detected flux by the frequency or wavelength bandwidth ($\Delta\nu$ or $\Delta\lambda$). Flux density is crucial in characterizing the spectral properties of sources.

For radio astronomy, flux density per unit frequency (S_ν) in janskys (Jy) is a commonly used unit:

$$1 \text{ Jy} = 10^{-26} \text{ W m}^{-2} \text{ Hz}^{-1}$$

2.1.5. Intensity

Intensity I_ν or I_λ , also known as specific intensity or surface brightness, is the flux density per unit solid angle. It measures the amount of energy radiated per second per unit area per unit solid angle of the source. Intensity is independent of distance and provides insights into the microscopic radiation processes of the emitting object.

The relationship between flux density and intensity is:

$$I_\nu = \frac{F_\nu}{\Omega}$$

where Ω is the solid angle subtended by the source. Intensity is commonly expressed in units of watts per square meter per hertz ($\text{W Hz}^{-1} \text{ m}^{-2} \text{ sr}^{-1}$) or watts per square meter per nanometer ($\text{W nm}^{-1} \text{ Hz}^{-1} \text{ m}^{-2} \text{ sr}^{-1}$) depending on the wavelength regime.

2.1.6. Relation between Intensity and Electric Field

Intensity is related to the electric field strength of the radiation waves via the Poynting vector. The intensity of radiation is proportional to the square of the electric field amplitude E_0 .

$$I_\nu \propto E_0^2$$

This relationship underscores the fundamental connection between the electromagnetic wave properties and the measurable quantities of radiation intensity.

In summary, astronomers employ various measures such as luminosity, flux, flux density, and intensity to quantitatively describe the amount of radiation emitted by astronomical sources. Each measure provides unique insights into the nature and properties of celestial objects across different wavelength regimes.

§2.2. Blackbody Radiation

At the start of the twentieth century, Max Planck's discovery that light's energy is quantized into packets called photons was pivotal. Blackbody radiation, the light emitted by a body that absorbs all incident light, is a key concept. This radiation helps us understand how hot objects cool by emitting light.

A blackbody is an idealized object that emits radiation solely based on its temperature, with no reflection or transmission. The interactions between photons and particles within the blackbody result in a thermal equilibrium, where both have the same temperature.

Photons are described by Bose–Einstein statistics, which help in determining the distribution of photon energies in thermal equilibrium. The energy distribution function of photons is directly related to the spectrum of emitted light, known as the Planck function:

$$B_\nu(T) = \frac{2h\nu^3}{c^2} \frac{1}{e^{h\nu/kT} - 1} \quad (2.2.1)$$

where:

- $h = 6.626 \times 10^{-34} \text{ J s} = 6.626 \times 10^{-27} \text{ erg s}$ is Planck's constant
- $k = 1.38 \times 10^{-23} \text{ J K}^{-1} = 1.38 \times 10^{-16} \text{ erg K}^{-1}$ is Boltzmann's constant
- c is the speed of light
- ν is the frequency of the observation
- T is the temperature of the radiating body in Kelvins

In the Planck function given in Equation (2.2.1), written as $B_\nu(T)$, the subscript ν indicates that the spectral measure is per unit frequency and B represents the intensity, or brightness, of the blackbody radiation and has units of intensity, $\text{W m}^{-2}\text{Hz}^{-1}\text{sr}^{-1}$. Since this is an intensity, the Planck function can also be expressed as flux per unit wavelength per steradian, which is denoted as $B_\lambda(T)$. Radio astronomers generally express the Planck function using $B_\nu(T)$. The equation for $B_\lambda(T)$ is

$$B_\lambda(T) = \frac{2hc^2}{\lambda^5} \frac{1}{e^{hc/\lambda kT} - 1} \quad (2.2.2)$$

It is very important to understand and appreciate that, even though B_ν and B_λ represent the same concept, they are not the same numerical quantity or even the same function. We discuss in more detail about the difference between these functions later in this section. We first discuss some important features of the Planck function.

Figures 2.1 and 2.2 display the log-log plots of these functions. Blackbody emission is a continuous spectrum that reaches zero at $\nu = 0$ (owing to the ν^3 term), increases to some peak value as ν increases, and then decreases and reaches zero again at $\nu = \infty$ (owing to the exponential term). Note that the Planck function depends only on the body's temperature and the frequency of the radiation. No other characteristic of the body is relevant. In other words, the intensity of radiation that a blackbody emits at any given frequency depends only on its temperature.

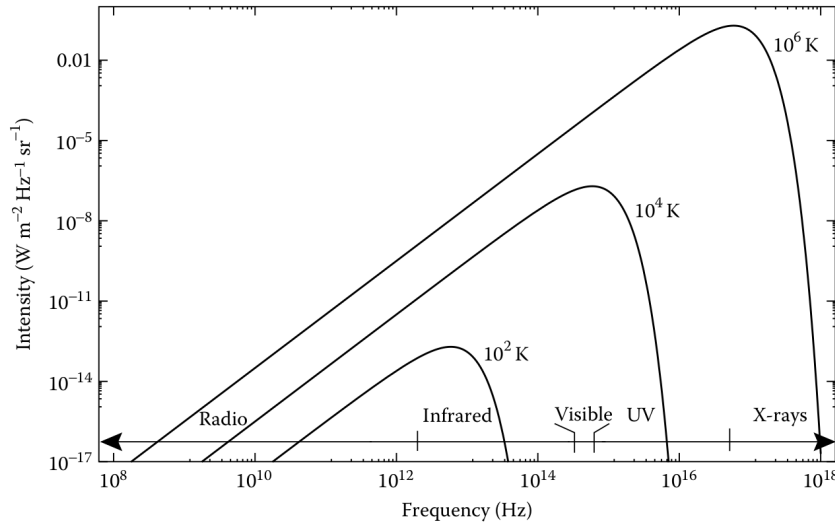


Figure 2.1: Log-log plot of $B_\nu(T)$ versus ν for three different temperatures.

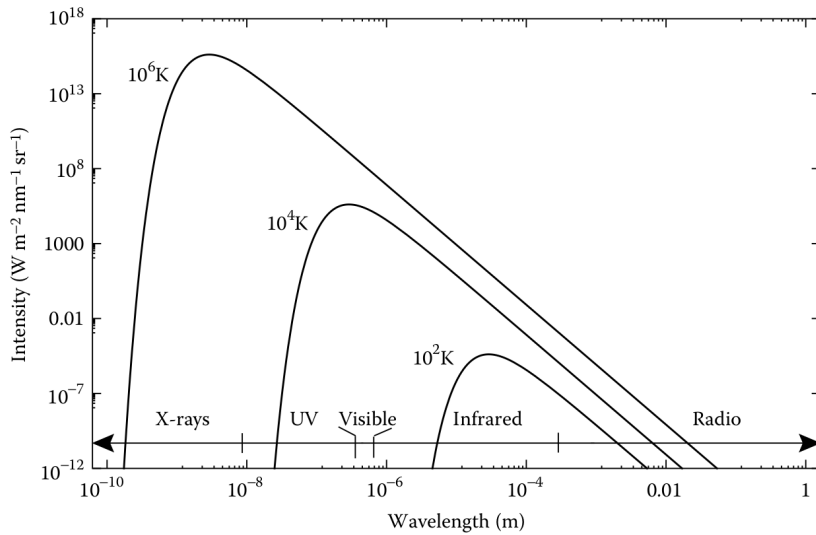


Figure 2.2: Log-log plot of $B_\lambda(T)$ versus λ for three different temperatures.

The total flux of radiation (W m^{-2}) emitted by the body can be obtained by integration of the Planck function over frequency and solid angle. The result shows that the total flux is given by

$$F = \sigma T^4 \quad (2.2.3)$$

where σ is the Stefan-Boltzmann constant. This is an expression of the Stefan-Boltzmann law. Another very useful result can be obtained by finding the frequency of the peak intensity of the Planck function. This frequency, ν_{\max} , is proportional to the body's temperature and is given by Wien's displacement law, which states

$$\nu_{\max} = 2.82 \frac{kT}{h}$$

Finally, it is also useful to calculate the brightness temperature of a source whose intensity is I_ν . This brightness temperature, T_B , is the temperature at which a blackbody would emit with an intensity equal to I_ν . That is, it is found by solving for T in the expression

$$I_\nu = B_\nu(T)$$

As mentioned above, radio astronomers typically express the Planck function using frequency (ν) rather than wavelength (λ). Radio astronomers also express the Planck function in a modified form using temperature units. The brightness temperature of a source whose specific intensity is I_ν is defined as the temperature of a blackbody that would emit the same specific intensity, T_B , at the frequency ν . The Planck function in the Rayleigh-Jeans approximation can be expressed as

$$B_\nu(T) \approx \frac{2\nu^2 kT}{c^2}$$

The brightness temperature of a source with intensity I_ν is then

$$T_B \approx \frac{I_\nu c^2}{2k\nu^2}$$

§2.3. Rayleigh-Jeans Approximation

At most radio wavelengths, the Planck function can be approximated by a much simpler expression, which makes for much easier math when using it. At most radio wavelengths, the frequency, ν , is so small that $\frac{\hbar\nu}{kT} \ll 1$ for any

reasonable temperature. The exponential in the denominator of the Planck function then can be approximated by a Taylor series expansion, yielding

$$\frac{1}{e^{h\nu/kT} - 1} \approx \frac{kT}{h\nu} \quad \text{for } \frac{h\nu}{kT} \ll 1 \quad (2.3.1)$$

and so,

$$B_\nu(T) \approx \frac{2h\nu^3}{c^2} \cdot \frac{kT}{h\nu} = \frac{2k\nu^2}{c^2} T \quad (2.3.2)$$

or

$$B_\nu(T) \approx \frac{2kT}{\lambda^2} \quad (2.3.3)$$

Note how simple this expression is in comparison to the Planck function (Equation (2.2.1)). This expression is very useful, provided you are in the realm where $\frac{h\nu}{kT} \ll 1$. This expression is known as the Rayleigh–Jeans approximation, often referred to as the Rayleigh–Jeans law.

§2.4. Brightness Temperature

Brightness temperature (T_B) is an important parameter in radio astronomy, providing a convenient way to describe the intensity of radiation using the Rayleigh–Jeans approximation. This approximation shows that at radio wavelengths, the intensity ($B_\nu(T)$) of radiation emitted by a blackbody is directly proportional to its temperature (T), i.e., $B_\nu(T) \propto T$.

At radio wavelengths, intensity and temperature of blackbody sources can be used interchangeably and are linearly related by $\frac{2k}{\lambda^2}$. In the Rayleigh–Jeans approximation, the brightness temperature is defined as:

$$T_B = \frac{\lambda^2}{2k} I_\nu$$

T_B is a property of the radiation, not the emitting object. For an opaque thermal source, T_B directly represents the object's temperature. However, it only equals the source's temperature when the source is both thermal and opaque.

At higher frequencies or lower temperatures, where $h\nu$ is not much smaller than kT , the Rayleigh–Jeans approximation is insufficient. In such cases, the full Planck function must be used:

$$I_\nu = B_\nu(T_B) = \frac{2h\nu^3}{c^2} \left(\frac{1}{e^{h\nu/kT_B} - 1} \right)$$

Brightness temperature measures intensity and equals the temperature of an opaque thermal source at low frequencies. For non-thermal radiation (e.g., synchrotron radiation), T_B is not related to the source temperature but still describes radiation intensity.

Temperature descriptions for intensity or radiation power also appear in other contexts, such as antenna temperature, noise temperature, receiver temperature, and system temperature, representing power per unit frequency in radio telescope observations.

§2.5. Coherent Radiation

The radio-wavelength radiation emitted by an individual electron is undetectable by any radio telescope; what we detect is the sum of emissions from many electrons. There are two main ways electromagnetic waves from different electrons can combine, which significantly affects how we treat the radiation mathematically and its physical properties.

Imagine a single electron oscillating at a fixed frequency, emitting electromagnetic waves at a single wavelength. If multiple wave chains, all in phase, join this initial chain, they amplify the initial wave constructively, resulting in coherent radiation. This is similar to what happens in a laser.

In contrast, incoherent radiation occurs when many unrelated electrons emit radiation independently, as in an incandescent light bulb. The resulting waves have random phases and cannot be modeled by a single chain of sine waves.

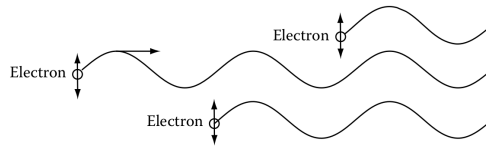


Figure 2.3: Creation of Coherent Radiation.

Mathematically, coherence of radiation means that at any location in space and time, the radiation has a specific phase. To understand coherence, consider two electromagnetic wave chains with identical frequencies and directions, but with a phase difference. Representing the waves as cosines:

$$E_1 = E_0 \cos(\omega t)$$

$$E_2 = E_0 \cos(\omega t + \Delta\phi)$$

Their sum is:

$$E_1 + E_2 = E_0 \cos(\omega t) + E_0 \cos(\omega t + \Delta\phi)$$

The intensity (I) is proportional to the square of the electric field, averaged over time. The intensity of each wave chain is:

$$I_1 = I_2 = \alpha E_0^2 / 2$$

The total intensity is:

$$I_{\text{total}} = \alpha(E_1 + E_2)^2 = \alpha E_0^2 [1 + \cos(\Delta\phi)]$$

When waves are in phase ($\Delta\phi = 0$), $\cos(\Delta\phi) = 1$, and the total intensity is four times that of an individual wave. For incoherent light, the interference term averages to zero, resulting in the total intensity being the sum of individual intensities.

In summary, incoherent light results in a total intensity equal to the sum of component intensities, while coherent light's intensity grows as the square of the sum of the component intensities. Despite the differing intensities, the total energies remain conserved, with coherent light having a higher intensity over a smaller wavelength range and a narrower beam.

§2.6. Interference of Light

Interference of light is crucial for understanding the functioning of radio telescopes. This concept was famously demonstrated by Thomas Young's double-slit experiment, which established the wave nature of light in the early nineteenth century.

The classroom demonstration typically uses a laser beam, which is highly coherent, shining on a double slit. The light from the slits combines to form an interference pattern on a screen. The pattern arises because the path lengths from the two slits to the screen differ, causing phase differences. At the midpoint between the slits, the path lengths are equal, so the phases are the same, resulting in constructive interference and a bright spot. At points offset from the midpoint, the path difference causes destructive interference, creating dark regions or nulls.

A schematic of Young's double-slit experiment and the resulting interference patterns is shown in Figure 2.4. Despite using sunlight, which is not coherent, Young observed interference patterns because he passed the sunlight through a pinhole before the slits, enhancing spatial coherence.

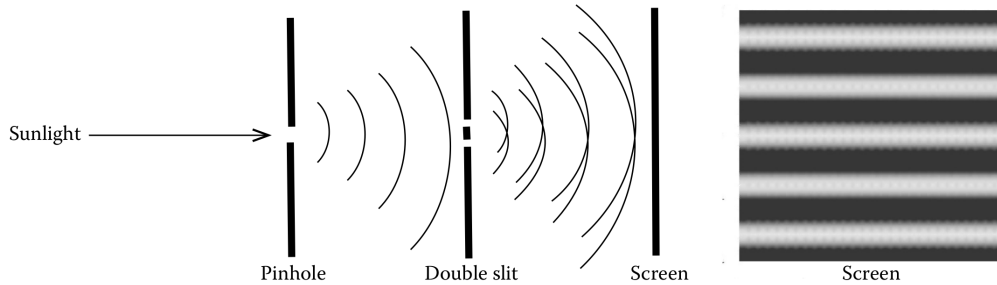


Figure 2.4: Schematic representation of Young's double-slit experiment is shown on the left and the display of the bright and dark lines that appear on the screen due to interference is shown on the right.

Interference patterns do not require all wave chains to be in phase. Each wave chain passing through the slits produces its own interference pattern. The total intensity pattern is the sum of these individual patterns. However, a range of frequencies or directions degrades the pattern, leading to partial coherence. Laser beams exhibit high spatial and temporal coherence, but no source is perfectly coherent.

Young used a pinhole to create wave fronts from a single point, ensuring high spatial coherence. Despite sunlight being blackbody radiation with all wavelengths, the human eye's limited wavelength sensitivity allowed Young to see the interference pattern, effectively filtering the light by wavelength.

Using coherent light sources in double-slit demonstrations simplifies observing well-defined nulls and peaks. However, understanding that partial coherence can still produce interference patterns is essential in radio astronomy. Observations involve a range of wavelengths and sources with finite spatial coherence, and the phases of the radiation are usually random. This understanding is crucial for appreciating the resolution limits of radio telescopes and the technique of interferometry or aperture synthesis.

§2.7. Polarization of Light

The direction of the electric field in an electromagnetic wave is described by its polarization. For waves traveling along the $+z$ -axis, the electric field (\vec{E}) oscillates perpendicular to the direction of travel, typically in the xy -plane, with the magnetic field (\vec{B}) perpendicular to both \vec{E} and the direction of travel.

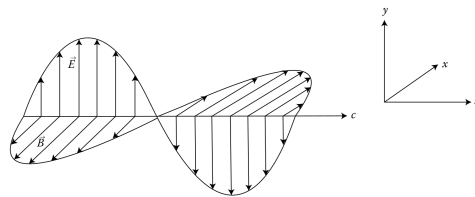


Figure 2.5: Propagation of plane electromagnetic waves along the z -axis with the electric field oscillating along the y -axis.

The electric field can oscillate in any direction within the xy -plane, affecting electrons differently based on their movement constraints. An electron constrained to move vertically will only be accelerated by vertically polarized waves.

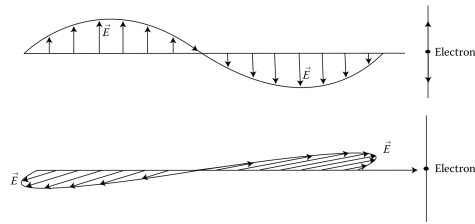


Figure 2.6: An electron moving vertically is accelerated by vertically polarized waves but unaffected by horizontally polarized waves.

Any electric field vector can be described by its components along the x - and y -axes (horizontal and vertical polarization).

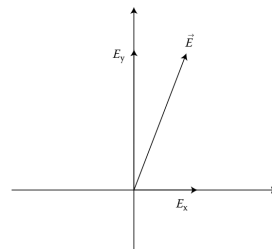


Figure 2.7: Total electric field vector described by its x - and y -components.

When the x - and y -components are out of phase, the total electric field vector rotates, leading to different polarization types:

1. **Linear polarization:** \vec{E} oscillates in a fixed direction.
2. **Circular polarization:** \vec{E} rotates with constant magnitude, describing a circle.
3. **Elliptical polarization:** \vec{E} describes an ellipse.

§2.8. Cosmic Microwave Background

The Cosmic Microwave Background (CMB) is the thermal radiation left over from the Big Bang. It is a faint glow of light that fills the universe in all directions. The CMB is a critical piece of evidence supporting the Big Bang theory and provides a wealth of information about the universe's early history.

The CMB was first discovered by Arno Penzias and Robert Wilson in 1965. They were conducting radio astronomy experiments using a horn antenna at Bell Labs in New Jersey when they detected an unexpected background noise. After ruling out all possible sources of interference, they realized they had discovered the CMB.

We use data from COBE [MCE⁺] Satellite to fit the Planck function to the CMB data. We fit the Planck function to the data and determine the temperature of the CMB. The Planck function is already defined in section 2.2.

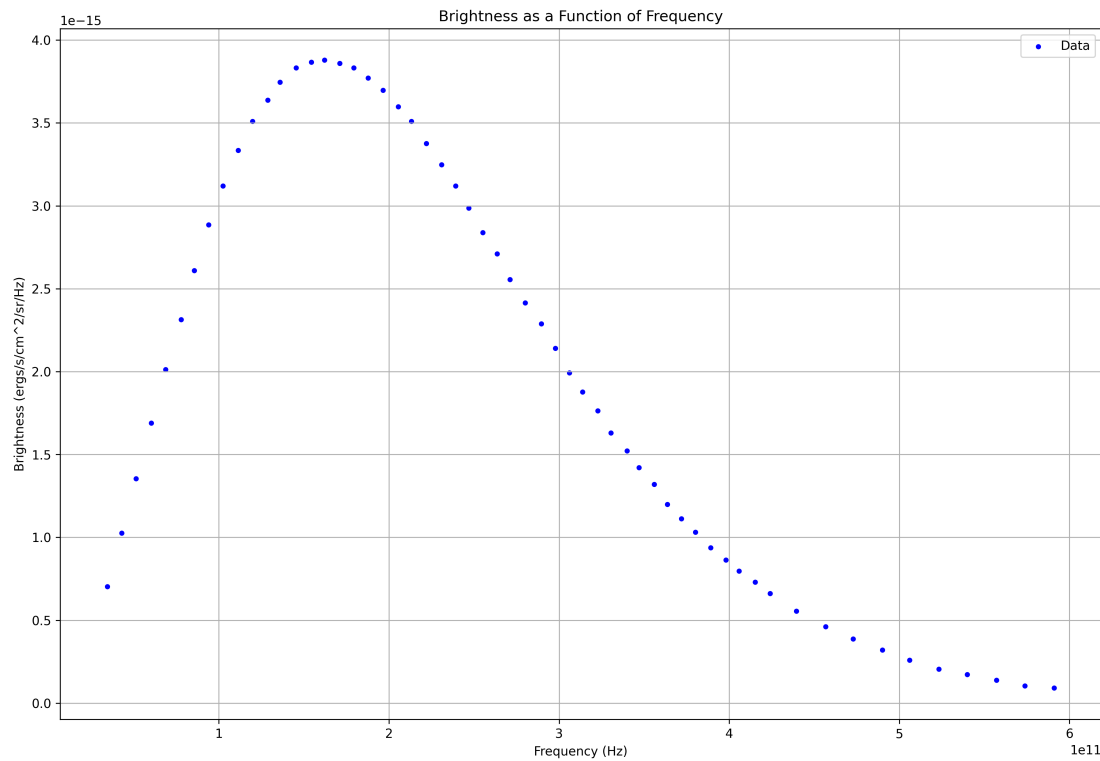


Figure 2.8: Plotted CMB Data

Using the blackbody function, we get the optimized CMB temperature to be **2.738305 K**.

§2.9. Hydrogen 21cm Line & Galaxy Rotation Curve

The Hydrogen 21cm line is a very important spectral line important in radio astronomy as it is used to study the distribution of neutral atomic hydrogen in the interstellar medium. The 21cm line is a hyperfine transition of the hydrogen atom, which occurs due to the spin-flip transition of the electron in the hydrogen atom. This line is important in studying the dynamics of galaxies and the distribution of hydrogen in the Universe.

The 21cm line is used to study the rotation curve of galaxies. The rotation curve of a galaxy is a plot of the orbital velocity of the stars and gas in the galaxy as a function of the distance from the center of the galaxy. The rotation curve of a galaxy is important in studying the mass distribution of the galaxy. The rotation curve of a galaxy is used to study the dark matter distribution in the galaxy.

To obtain the galaxy rotation curve, we will use synthetic spectra available for different spectrums of different distance intervals within that is a Hydrogen 21 cm line at a Doppler velocity. We fit for the Doppler velocity of the 21 cm line for each distance. To do so, we fit a gaussian to the spectral line and determine the central frequency. We use the displacement from the expected value to find the velocity. Once all lines are done, plot the velocities as a function of distance from the centre of our galaxy.

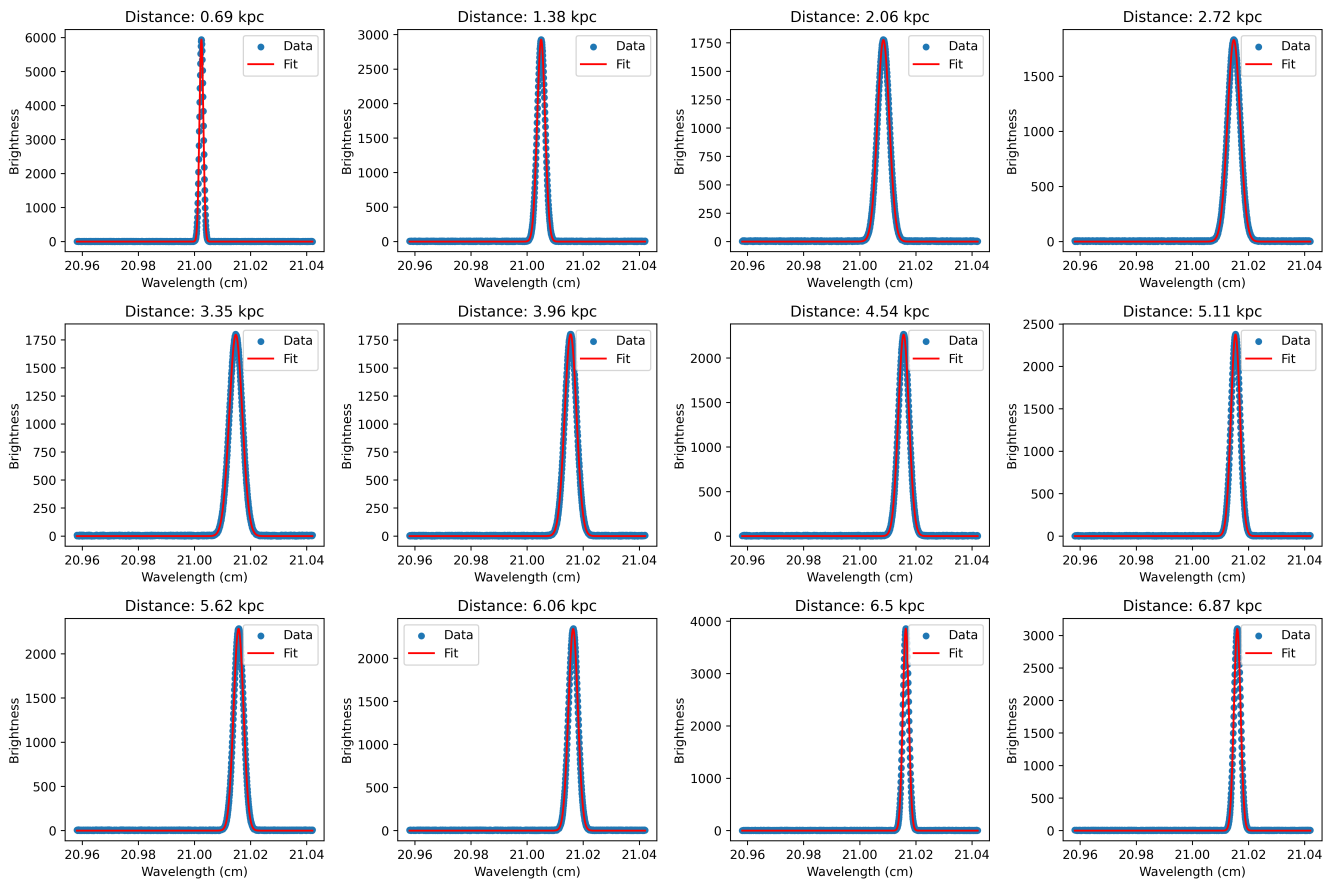


Figure 2.9: Plots for each distance

Using the data obtained from the Gaussian fits, we can plot the velocities as a function of distance from the centre of the galaxy.

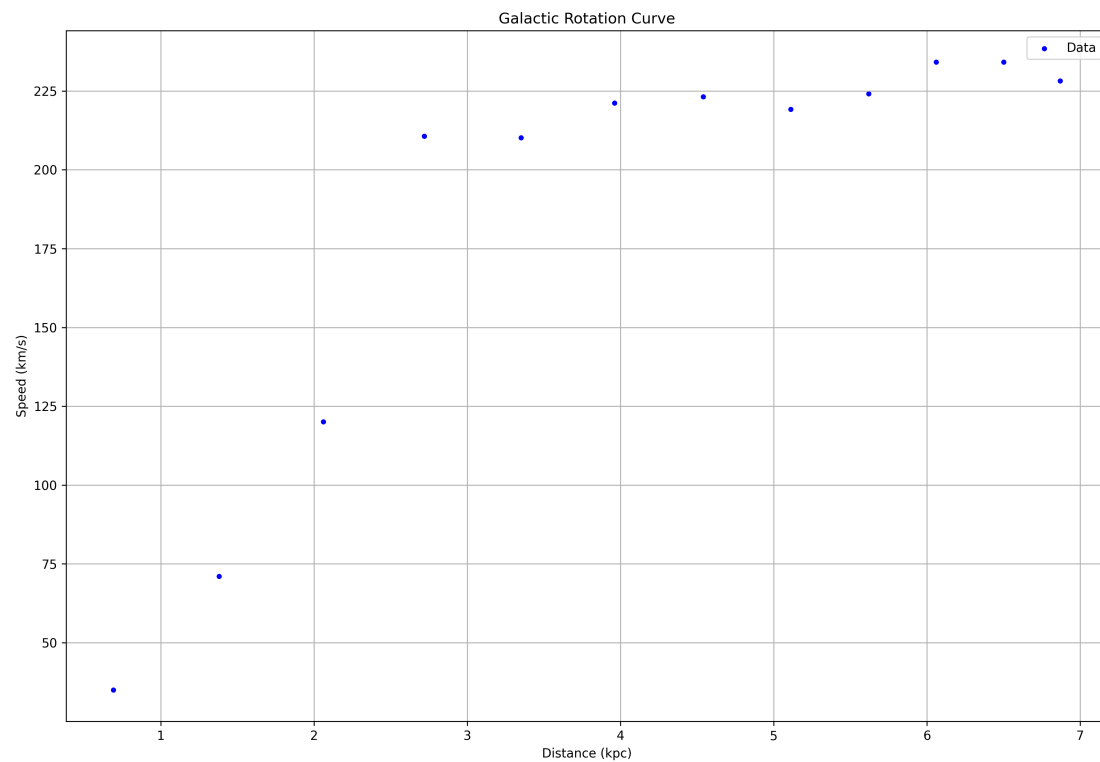


Figure 2.10: Galaxy Rotation Curve

Chapter 3

Radio Telescopes

Bibliography

- [CIR24] CIRADA. Cirada cutout service, 2024.
- [Kc24] Mooley Kunal and collaborators. Gw170817 afterglow data, 2024.
- [KHK20] John D. Kraus, Gerald M. Heiligman, and Timothy Koch. *Fundamentals of Radio Astronomy: Observational Methods*. CRC Press, Boca Raton, FL, 2nd edition, 2020.
- [MCE⁺] J. C. Mather, E. S. Cheng, R. E. Eplee, Jr., R. Isaacman, R. A. Shafer, J. M. Weisberg, and E. L. Wright. A preliminary measurement of the cosmic microwave background spectrum by the Cosmic Background Explorer (COBE) satellite.
- [NAS24] NASA/GSFC. Flexible image transport system (fits), 2024.